High-energy lithium batteries based on single-ion conducting polymer electrolytes and Li[Ni0.8Co0.1Mn0.1]O2 cathodes

Zhen Chen, Dominik Steinle, Huu-Dat Nguyen, Jae-Kwang Kim, Alexander Mayer, Junli Shi, Elie Paillard, Cristina Iojoiu, Stefano Passerini, Dominic Bresser

High-Energy Lithium Batteries based on Single-Ion Conducting Polymer Electrolytes and $Li[Ni_{0.8}Co_{0.1}Mn_{0.1}]O_2$ Cathodes

Zhen Chen[a,b], Dominik Steinle[a,b], Huu-Dat Nguyen[c,§], Jae-Kwang Kim[d], Alexander Mayer[a,b], Junli Shi[e,f], Elie Paillard[e], Cristina Iojoiu[c,g],* Stefano Passerini[a,b],* and Dominic Bresser[a,b]*

[a] Helmholtz Institute Ulm (HIU), 89081 Ulm, Germany

[b] Karlsruhe Institute of Technology (KIT), 76021 Karlsruhe, Germany

[c] Univ. Grenoble Alpes, Univ. Savoie Mont Blanc, CNRS, Grenoble INP (Institute of Engineering Univ. Grenoble Alpes), LEPMI, UMR5279, 38000 Grenoble, France

[d] Department of Solar & Energy Engineering, Cheongju University, Cheongju, Chungbuk 28503, Republic of Korea

[e] Helmholtz Institute Muenster, Forschungszentrum Juelich (IEK 12), 48149 Muenster, Germany

[f] Advanced Li-ion Battery Engineering Laboratory and Key Laboratory of Graphene Technologies and Applications of Zhejiang Province, Ningbo Institute of Materials Technology & Engineering, Chinese Academy of Sciences, Zhejiang 315201, P. R. China

[g] Réseau sur le Stockage Electrochimique de l'Energie (RS2E), CNRS, FR3459, 80 039 Amiens Cedex, France

*** Corresponding authors:**

dominic.bresser@kit.edu (D. Bresser); stefano.passerini@kit.de (S. Passerini); cristina.iojoiu@lepmi.grenoble-inp.fr (C. Iojoiu)

[§] **Present affiliation:** Laboratoire Matériaux Batteries (LM)/STB/DEHT/LITEN, CEA Grenoble, 17 avenue des Martyrs, 38000 Grenoble, France

ABSTRACT

Single-ion conducting polymer electrolytes are considered ideal for suppressing dendritic lithium deposition, but so far suffered instability at elevated potentials and, thus, incompatibility with next-generation high-energy cathodes such as Ni-rich $Li[Ni_{1-x-y}Co_xMn_y]O_2$ ($NCM_{(1-x-y)xy}$).

Herein, we show that the thoughtful design of electrolytes based on multi-block co-poly(arylene ether sulfone)s and incorporating suitable "molecular transporters" (such as propylene carbonate) may, in fact, enable the realization of high-energy lithium-metal batteries employing, for the first time, NCM_{811}-based positive electrodes. These batteries can be cycled with high reversible capacity at various temperatures, including 20 °C and even 0 °C, for more than 500 cycles without substantial capacity fading when applying an optimized charging mode. The careful electrochemical characterization and *ex situ* investigation of the electrode/electrolyte interfaces reveals, moreover, that the use of such single-ion conductor successfully inhibits dendritic lithium metal deposition, while particular care has to be taken for the interface between the electrolyte and the NCM_{811} cathode.

Keywords: single-ion conductor; polymer electrolyte; NCM_{811}; cathode; lithium battery

1. Introduction

Lithium-ion batteries have achieved great success for powering portable devices and are increasingly employed also for large-scale applications such as (hybrid) electric vehicles and stationary energy storage [1–3]. Nonetheless, further improvement is needed – specifically for the latter applications – targeting enhanced energy and power densities as well as safety [3–6]. For an increase in energy density, the use of metallic lithium as the negative electrode is considered the "next big thing" thanks to its very high gravimetric and volumetric capacity of 3862 mAh g^{-1} and 2047 Ah L^{-1}, respectively, in combination with the ultimately low redox potential of -3.04 V *vs.* the standard hydrogen electrode (SHE) [7–9]. However, the continuous reaction with common liquid organic electrolytes, resulting in the formation of a steadily increasing amount of "dead" lithium and drying-out of the cell, in addition to the severe risk of dendritic lithium deposition [6, 8–10] have so far inhibited the commercial implementation of lithium metal anodes. Differently, the combination with polymer-type electrolytes based on poly(ethylene oxide) (PEO) has been commercialized already and found application in electric vehicles [6]. As the ionic conductivity at ambient temperature is rather low, though, with about 10^{-5} to 10^{-4} S cm^{-1} (compared with 10^{-3} to 10^{-2} S cm^{-1} for liquid organic electrolytes), the battery cells comprising such electrolytes have to be operated (during discharge and charge!) at elevated temperatures of ca. 60 °C [11–13]. Moreover, the relatively low Li^+ transference number (t_{Li}^+ = 0.1 to 0.5) of such dual-ion conducting polymer electrolytes induces severe issues for the long-term stable cycling; specifically, the formation of an ionic concentration gradient that leads to substantial polarization in case of high dis-/charge rates and an uneven (dendritic) lithium deposition [14–19]. To overcome such issues, the immobilization of the anionic charge to the polymer has emerged as a valid strategy, exhibiting a t_{Li}^+ of (close to) unity, but the ionic conductivity at room temperature remained well below the

conductivity of liquid electrolytes with about 10^{-7} to 10^{-5} S cm^{-1} [16, 20–22]. Even though one has to consider that these conductivity values reflect essentially the mobility of the lithium cation in contrast to dual-ion conducting electrolytes for which more than 50% of the determined conductivity are originating from the anion mobility, higher conductivities are required. Recently, single-ion polymer electrolytes additionally incorporating liquid organic carbonates such as ethylene carbonate (EC) and dimethyl carbonate (DMC) have been reported with conductivity values of up to 10^{-3} S cm^{-1} at room temperature [13, 23–26]. However, the addition of mechanically stabilizing polymers like poly(vinylidene difluoride) (PVdF) or its hexafluoropropylene-copolymer (PVdF-HFP) is required [13, 23, 24, 26]. More importantly with respect to the achievement of high energy densities, all these studies remained limited to the utilization of $LiFePO_4$ as cathode active material due to the limited electrolyte stability towards oxidation. Very recently, some of the authors reported the synthesis and electrochemical characterization of a single-ion conducting polymer electrolyte based on multi-block co-poly(arylene ether sulfone) functionalized with lithium perfluorosulfonimide side chains [27]. When doped with EC, which selectively coordinates the ionophilic block, such self-standing electrolyte membranes (thanks to the mechanical stability of the ionophobic block) provide a remarkable ionic conductivity of about 10^{-3} S cm^{-1} at 30 °C. Moreover, the chemical design of the polymer allowed for the stable cycling of $Li[Ni_{1/3}Co_{1/3}Mn_{1/3}]O_2$ (NCM_{111}) cathodes for more than 200 cycles without any significant capacity fading. The specific capacity, however, remained limited to about 100 mAh g^{-1} at C/5 and 40 °C due to the anodic cut-off potential of 4.2 V *vs.* Li/Li^+ and, presumably, the limited penetration of the rather rigid polymer into the pores of the positive electrode.

Herein, we addressed these issues by modifying the length and ratio of the ionophilic and ionophobic block and replacing EC by propylene carbonate (PC), which has a relatively lower melting point (ca. -49 °C *vs.* 36 °C), targeting an increased flexibility and higher charge carrier concentration of the polymer to enable facile electrode wetting and suitable charge transfer at the electrode/electrolyte interface. Moreover, the replacement of EC is considered to be beneficial for the electrochemical stability towards oxidation [28–30]. As a result, we obtained excellent cycling stability of high-energy next generation $Li[Ni_{0.8}Co_{0.1}Mn_{0.1}]O_2$ (NCM_{811}) cathodes at 40 °C, 20 °C, and even 0 °C and anodic cut-off potentials as high as 4.5 V. To the best of our knowledge, this is the first report on a (single-ion conducting) polymer electrolyte with such remarkable performance and in combination with NMC_{811} cathodes, rendering it a highly promising candidate for the realization of safe high-energy lithium-metal batteries.

2 Experimental section

2.1 Sample preparation

The general synthesis of the partially fluorinated multi-block co-poly(arylene ether sulfone) bearing lithium perfluorosulfonimide side chains attached to the ionophilic polyethersulfone (PES) blocks which form the polymer backbone together with the fluorinated polyethersulfone (FPES) ionophobic blocks (Fig. 1a) has been reported earlier [27] and is described in brief in the Supporting Information (see also Fig. S1, Fig. S2, as well as Tab. S1 and Tab. S2). Herein, we modified the length of these two blocks and their ratio *i.e.*, from 15/15 to 10/5 by simply adjusting the amount of monomers building up the two blocks, accordingly. Subsequently, the resulting polymer powder was swollen with 70 wt% PC to obtain a less gum-like material. This compound was sandwiched between two Mylar foils and pressed in order to obtain translucent thin

membranes (denoted as SI10-05-70%PC; see Fig. 1b). The whole processing was performed in a dry room with a dew point of less than -70 °C. The NCM_{811} electrodes were prepared by dispersing 92 wt% of NCM_{811}, 4 wt% of Super C65 (TIMCAL) and 4 wt% of poly(vinylidene difluoride) (PVdF, Solvay) in an appropriate amount of *N*-methyl-2-purrolidone (NMP, Aldrich) to obtain a homogeneously dispersed slurry that was subsequently cast on aluminum foil using the doctor-blade technique. The pre-dried electrodes were punched into disks (∅ = 12 mm), which were subsequently dried at 100 °C for 12 h under vacuum, before being pressed at 10 tons for 10 s to increase the electrode density. The active material mass loading was about 2.0 ± 0.2 mg cm^{-2}. The complete processing was performed in a dry room with a dew point well below -60 °C.

2.2 *Physicochemical characterization*

The ion-exchange capacity (IEC; meq. Li^+/g) of the SI10-05 ionomer was determined from both ^{19}F NMR spectra and acid-base titration of the acidified ionomer membranes. Size exclusion chromatography with multiangle light scattering (SEC-MALS) analysis was performed using a Waters 590 GPC equipped with a Waters 410 differential refractometer and a Waters 745 Data Module at ambient temperature using a 1M solution of $NaNO_3$ in dimethylformamide (DMF) with a flow rate of 1 mL min^{-1}. A 1 wt% solution of the ionomer was filtered through a 0.45 mm Millipore PTFE filter into the columns. The calibration was performed using polystyrene standards. A qualitative study of the mechanical properties and elasticity of the polymer membranes (including PC) was conducted by repeatedly stretching it and subsequently allowing it to relax (Video S1). For the determination of the transference number (t^+), pulsed-field gradient nuclear magnetic resonance spectroscopy (PFG-NMR) was performed using a 9.4 T Bruker Advance 400 with a diffusion probe of 5 mm and using a stimulated echo sequence. For this purpose, the

SI10-05-70%PC membranes were cut into pieces and introduced into the NMR tube (diameter 4 mm), which was sealed inside the glovebox. The determination of lithium-ion transference number (t^+) was based on the measurement the self-diffusion coefficients of Li (D_{Li}) and F (D_F) at 30 °C. The thermal stability of the dry SI10-05 powder and the SI10-05-70%PC membranes was analyzed via thermogravimetric analysis (TGA; TA Instrument Discovery, Model Q2000). The TGA was performed at a heating rate of 3 K min^{-1} in a temperature range of 40 to 800 °C under an artificial air flow of 25 mL min^{-1} (N_2: 18.75 mL min^{-1}; O_2: 6.25 mL min^{-1}). The morphology of the fresh and cycled metallic lithium (Honjo) as well as the fresh and cycled NCM_{811} electrodes was investigated by scanning electron microscopy (SEM; ZEISS EVOMA10 microscope). For the *ex situ* characterization, the cells were disassembled in a dry room to recover the single electrodes. To remove the comprised PC, the electrodes were vacuum dried by a mechanical pump and afterwards a turbo-molecular pump (10^{-9} Bar), before transferring them into the SEM using a self-designed transfer box to avoid any contact with air and moisture. For a qualitative evaluation of the safety of the PC-comprising membrane, we subjected these several times to a candle flame (Video S2). For comparison, we conducted the same experiment with a Whatman glass fiber separator (thus, avoiding any impact of the separator itself) drenched with a 1M solution of LiTFSI (lithium bis(perfluoromethanesulfonyl)imide; 3M) in PC (Video S3).

2.3 *Electrochemical characterization*

The limiting current density of the electrolyte was determined in two-electrode pouch cells, which were assembled by sandwiching a SI10-05-70%PC membrane between two Li foils (Honjo) in a dry room. The cells were aged in a temperature-controlled climatic chamber (Binder) at varying temperatures (-10, 0, 20, and 40 °C) for 6 h prior to the measurements, which were

performed at a sweep rate of 0.02 mV s^{-1} using a Solatron 1400 CellTest system. The electrochemical stability window (ESW) was determined as well in two-electrode pouch cells assembled in a dry room. For these measurements, a nickel and a lithium foils were used, serving as working and counter electrode, respectively. Fresh cells were used for each experiment. The cells were aged in a climatic chamber (Binder) at 20 °C for 6 h before conducting linear sweep voltammetry (LSV) using VMP instrument with a sweep rate of 0.02 mV s^{-1}. Additional cyclic voltammetry tests (sweep rate: 0.5 mV s^{-1}; temperature: 20 °C; VMP Biologic) of asymmetric Ni/SI10-05-70%PC/Li pouch cells were performed in different voltage ranges, *i.e.*, 0.0 V to 3.0 V and 3.0 V to 4.7 V to further investigate the electrochemical stability towards reduction and oxidation, respectively. Cyclic voltammetry experiments on Li/NCM_{811} full-cells were performed in two-electrode Swagelok-type cells in a voltage range of 3.0 V to 4.3 V at a scan rate of 0.02 mV s^{-1} for first three cycles, followed by 50 continuous cycles at 0.2 mV s^{-1} (20 °C; VMP Biologic). EIS spectra of Li/NCM_{811} full-cells were measured at delithiation state (4.3 V) and lithiation state (3.0 V) upon galvanostatic cycling (current density: 1C, 180 cycles) in the same VMP instrument (frequency range: 100 kHz 100 mHz; AC amplitude: 10 mV; temperature: 20 °C). Galvanostatic cycling of Li/NCM_{811} full-cells was performed using a Maccor 4000 battery tester employing two-electrode Swagelok-type cells. A dis-/charge rate of 1C corresponds to a specific current of 180 mA g^{-1}.

3. Results and discussion

3.1 Characterization of SI10-05-70%PC electrolyte

While we kept the general polymer chemistry the same as in our previous study [27], we intentionally reduced the length of the two blocks and increased the relative share of the ionophilic

block in order to increase the flexibility and ductility of the polymer while simultaneously increasing the lithium cation concentration. Expressed in Fig. 1a, the average block lengths for the backbone being composed of the PES block, bearing the lithium perfluorinated sulfonimide function, and the FPES block were 10 kg mol^{-1} and 5 kg mol^{-1}, respectively. The resulting ionomer is hereinafter referred to as SI10-05. The lithium concentration was 1.15 ±0.03 mol kg^{-1} as determined by IEC analysis (Supplementary Tab. S2). In total, the mass of the ionomer sums up to an average molecular weight (M_w) and number average molecular weight (M_n) of 362 kg mol^{-1} and 165 kg mol^{-1}, respectively, with a polydispersity index (I_p) of 2.2 (Supplementary Tab. S3). The lithium transference number (t^+) was determined by PFG-NMR to be 1, based on the recorded self-diffusion coefficients of lithium (D_{Li} = 0.31±0.01×10^{-10} m^2 s^{-1}) and fluorine (D_F: no measurable diffusion). Fig. 1b displays typical translucent thin membranes of SI10-05-70%PC after swelling with 70 wt% of PC. In Video S1, a piece of SI10-05-70%PC was subjected to repeated stretching, revealing high elasticity and suitable mechanical properties. Regarding the thermal stability, in the dry state, the ionomer is stable up to about 350 °C, before a significant weight loss is observed in the TGA data (Supplementary Fig. S3). The evaporation of incorporated PC occurs above 100 °C and until about 240 °C. The polymer decomposition, however, remains unaffected by the introduction of PC, rendering this electrolyte very stable – especially in comparison with liquid organic electrolytes containing $LiPF_6$ as conducting salt, which decomposition occurs at around 70 °C [31]. In fact, a qualitative evaluation of the flammability and ignition of such PC-imbibed electrolyte membrane by subjecting it several times to a candle flame (Video S2) reveals that these membranes do not burn (apart from some (evaporating) PC at the surface), which is ascribed to the self-extinguishing properties of the (fluorinated) polyethersulfone backbone [27, 32–34]. Differently, a glass fiber separator drenched with

1M LiTFSI in PC is easily ignited and keeps burning until all electrolyte has been consumed (Video S3). This brief comparison highlights the inherent safety of this single-ion polymer electrolyte.

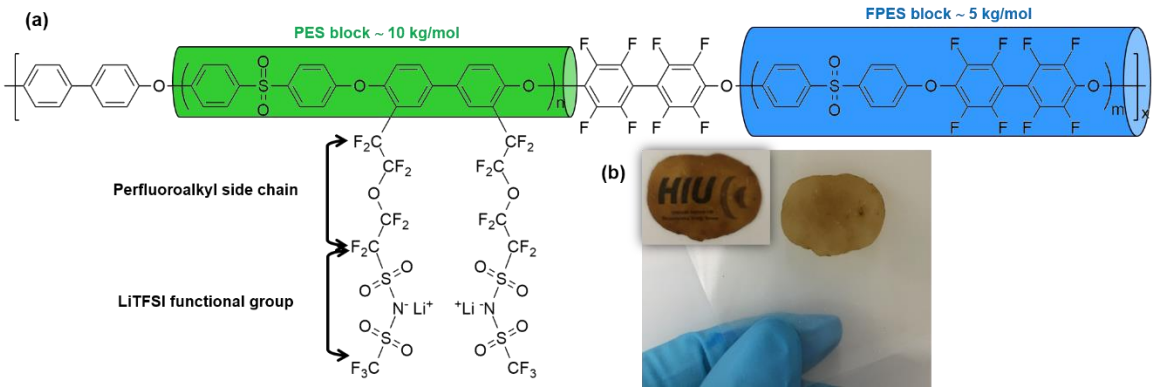

Fig. 1. a) Molecular architecture of the SI10-05 ionomer with the ionophilic PES block highlighted in green and the ionophobic FPES block highlighted in blue. b) Photographs of the SI10-05-70%PC ionomer membranes after the pressing between two Mylar foils.

3.2 Physicochemical and electrochemical properties of SI10-05-70%PC electrolyte

The ionic conductivity of the SI10-05-70%PC electrolyte in the temperature range of -30 °C to 90 °C is presented in Fig. 2a. The plot reveals a typical Vogel–Tammann–Fulcher (VTF), which indicates that the Li^+ cation transport is related to the solvent-coordinated transport, meaning that the PC solvent molecules are serving as a kind of "molecular transporter", presumably supported by the mobility of the ionic side chains. Remarkably, the ionic conductivity exceeds 1 mS cm^{-1} at 40 °C, which is comparable to or even higher than earlier reported single-ion conductors comprising organic solvents [35–40]. At 20 °C, the conductivity is rather high (about 0.6 mS cm^{-1}) considering that this value originates solely from the mobility of the Li^+ cation. In order to get the full picture for the charge transport within the electrolyte membrane, the limiting current density

(j_0) was also determined at various temperatures (Fig. 2b). As anticipated, the obtained value is substantially higher than in our previous work for the SI15-15-55%EC electrolyte system (*i.e.*, 1.2 mA cm^{-2} at 50 °C) [27] with 1.32 mA cm^{-2} and 1.57 mA cm^{-2} at 20 °C and 40 °C, respectively, due to the increased Li^+ concentration and the ratio of the conducting phase. Also at 0 °C and even -10 °C, the limiting current density is still rather high with about 0.41 mA cm^{-2} and 0.33 mA cm^{-2}, respectively, suggesting for decent to good performance even at relatively low temperatures.

In a next step, we evaluated the electrochemical stability of the SI10-05-70%PC electrolyte system. The results are presented in Fig. 2c–f with the determination of the electrochemical stability window shown in Fig. 2c. The peak at around 1.3 V during the cathodic scan is assigned to the reductive decomposition of PC [41], potentially including a minor contribution from residual DMSO from the synthesis [42]. In fact, conducting cyclic voltammetry in the cathodic sweep range of 0.0 V to 3.0 V (Fig. 2e) shows that this initial peak disappears after the first cathodic sweep (note a slight shift to lower voltage due to the faster sweep rate) vanishes, indicating a stabilized electrode/electrolyte interface. From the second cycle onwards, however, two very minor new peaks are observed at about 1.4 V and 0.5 V, which have probably been superimposed earlier by the solvent decomposition. According to a study by Kim *et al.* [43], these reduction peaks can be assigned to the reaction of Li^+ and NiO_x on the surface of the Ni foil, as also suggested by the accompanying oxidation peaks at around 1.0 V and 2.4 V, which are stabilizing after three CV cycles. The anodic sweep in Fig. 2c reveals two small oxidation peaks at around 4.5 V to 4.6 V, well evident in Fig. 2d, which are as well assigned to the decomposition of PC and potentially remaining DMSO [44, 45].

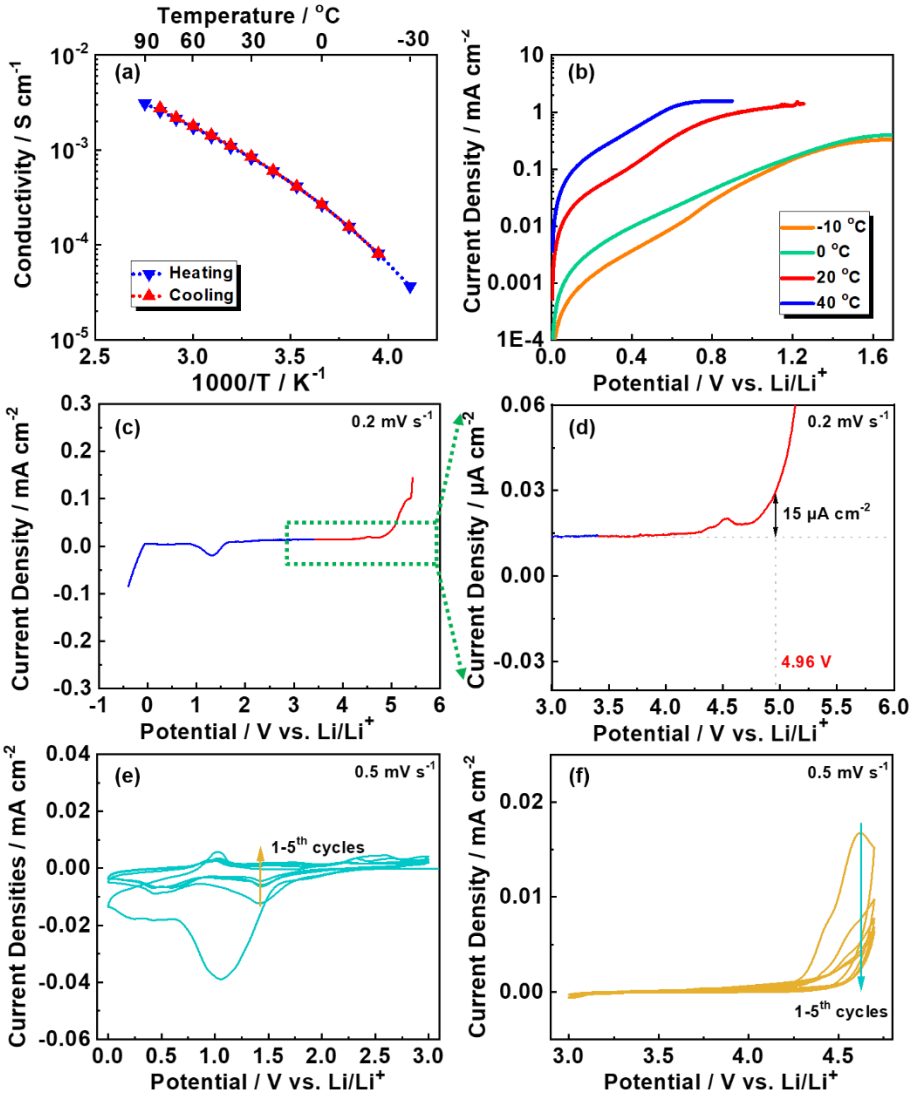

Fig. 2. a) Ionic conductivity of the SI10-05-70%PC electrolyte as a function of temperature. The ionic conductivity was recorded upon heating and cooling to confirm the reversibility of this analysis. b) Determination of the limiting current density at various temperatures. c) Determination of the electrochemical stability window of the SI10-05-70%PC electrolyte membranes via linear sweep voltammetry (sweep rate: 0.2 mV s^{-1}). d) Magnification of the anodic sweep as indicated by the dotted green frame in panel c) with an exemplary determination of the oxidative stability by choosing 15 µA cm^{-2} as the maximum evolving current. e,f) Cyclic voltammetry studies towards e) reduction in a voltage range of 0.0 V to 3.0 V and f) oxidation within a voltage range of 3.0 V to 4.7 V (sweep rate: 0.5 mV s^{-1}; note the different scale compared to panel c), especially for the current density).

Also in this case, the further investigation *via* cyclic voltammetry in the voltage range of 3.0 V to 4.7 V (Fig. 2f) indicates that the electrode/electrolyte interface is stabilizing upon cycling, as the evolving current is steadily decreasing to essentially 0 mA cm^{-2} up to 4.5 V. Setting an exemplary limit of 15 μA cm^{-2} for the evolving current for the determination of the anodic stability would mean that it is as high as 4.96 V (Fig. 2d), even though such a value must be taken with care given the fact that it is determined on a flat Ni electrode. Overall these results support for the implementation of the electrolyte in lithium-metal batteries comprising Ni-rich NCM cathodes.

3.3 Electrochemical behavior of SI10-05-70%PC electrolyte in Li/NCM_{811} full-cells

To start with, we evaluated Li/NCM_{811} cells *via* cyclic voltammetry (Fig. 3). The initial three CV cycles at a sweep rate of 0.02 mV s^{-1} in a voltage range of 3.0 V to 4.3 V are shown in Fig. 3a. Three typical redox pairs are observed associated to the hexagonal and monoclinic (H1 ↔ M), monoclinic and hexagonal (M ↔ H2), and hexagonal and hexagonal (H2 ↔ H3) phase transitions [46, 47]. The two, high-voltage pairs are perfectly overlapping upon cycling, indicating for the high reversibility of the associated phase transitions. Regarding the first redox couple (associated with the H1 ↔ M phase transition), a slight shift of the anodic peak towards lower potentials is noted, resulting in a decreasing separation of the redox peaks (ΔV) from 0.134 V to 0.085 V and, eventually, 0.066 V in the third cycle. It is worth mentioning that the ΔV in the third cycle is approaching the theoretical value of 0.059 V for a reversible electron transfer reaction [48, 49], which is very impressive for a polymer electrolyte cell. In a subsequent step, the same cell was subjected to 50 continuous CV cycles at a higher sweep rate of 0.2 mV s^{-1} (Fig. 3b). At such relatively higher sweep rate, the redox peak couples for the second and third phase transitions

(*i.e.*, M ↔ H2 and H2 ↔ H3) are less distinguishable. Furthermore, we observed a slightly increased polarization, evidenced by the higher redox peak separation. Nevertheless, the redox peak separation (ΔV) of H1 ↔ M gradually decreased and maintained stable after about 25 cycles. In addition, the redox peak intensity remained almost unchanged after the initial three cycles, confirming the good reversibility of the electrochemical reactions occurring.

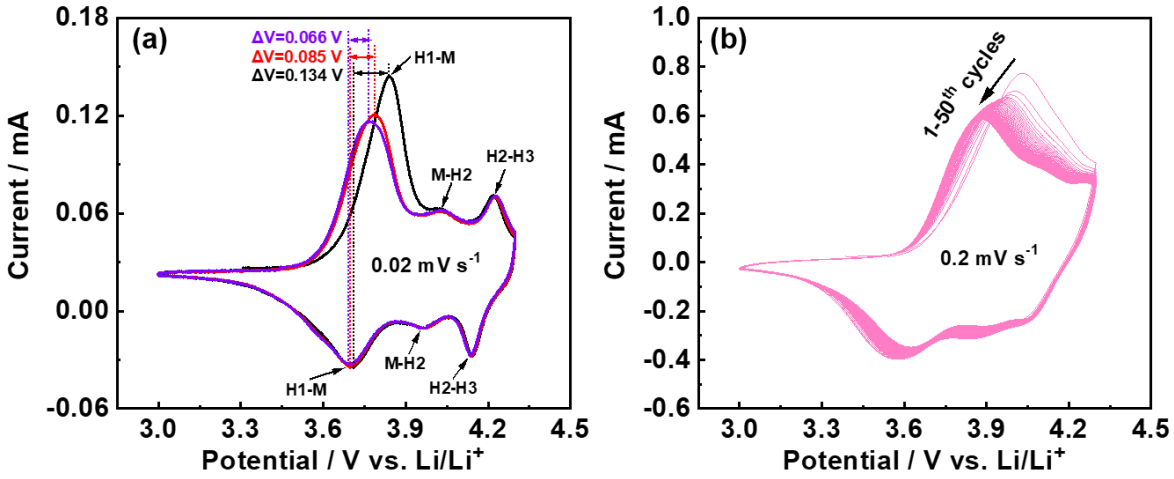

Fig. 3. Cyclic voltammetry conducted in a voltage range from 3.0 V to 4.3 V: a) Three cycles at a sweep rate of 0.02 mV s^{-1}; b) 50 consecutive CV cycles at a sweep rate of 0.2 mV s^{-1}.

3.4 Galvanostatic cycling and rate capability

Keeping the voltage range constant, we evaluated in a next step the rate capability and long-term constant current cycling performances of Li/NCM_{811} cells comprising the SI10-05-70%PC electrolyte at 20 °C and 40 °C (Fig. 4). In the first cycle, at 0.05C and 20 °C, the Li/NCM_{811} cell delivered a reversible discharge capacity of 201 mAh g^{-1} (Fig. 4a), which is very close to the reversible discharge capacity of about 203 mAh g^{-1} at 0.1C and 20 °C obtained for the same electrode combination with a standard liquid organic electrolytes (Supplementary Fig. S4). An even higher discharge capacity of around 206 mAh g^{-1} was recorded for the Li/SI10-05-

70%PC/NCM_{811} cell at 0.05C and 40 °C (Fig. 4b), presumably due to the enhanced kinetics at such elevated temperature. On the contrary, the first-cycle Coulombic efficiency was higher at 20 °C than at 40 °C with 90.6% *vs.* 81.1% as a result of extended irreversible side reactions at elevated temperatures. Indeed, as apparent already from the first cycle, the enhanced kinetics are advantageous for the achievable capacity – specifically at elevated dis-/charge rates – but disadvantageous in terms of Coulombic efficiency – also upon continuous cycling (Fig. 4a–c). At 40 °C the reversible specific capacity is 196 mAh g^{-1} at 0.1C, 183 mAh g^{-1} at 0.2C, 177 mAh g^{-1} at 0.5C, 165 mAh g^{-1} at 1C, 148 mAh g^{-1} at 2C, and 91 mAh g^{-1} at 5C. At 20 °C it is somewhat lower with 191 mAh g^{-1} at 0.1C, 180 mAh g^{-1} at 0.2C, 162 mAh g^{-1} at 0.5C, 139 mAh g^{-1} at 1C, 106 mAh g^{-1} at 2C, and 38 mAh g^{-1} at 5C. The subsequent long-term cycling stability, however, is better at 20 °C with 80% capacity retention after 443 cycles at 0.5C compared to 320 cycles at 0.5C and 40 °C thanks to the higher average Coulombic efficiency of 99.8% (20 °C) compared to 98.8% (40 °C). The superior cycling stability is also well reflected by an additional test, for which we cycled fresh cells constantly at 1C for 180 cycles after the formation at 0.05C and 0.1C (Fig. 4d). The Li/SI10-05-70%PC/NCM_{811} cell cycled at 20 °C revealed an exceptional capacity retention of 97.2% after this test compared to 80.4% for the cell cycled at 40 °C. While the latter cell showed a higher initial capacity of about 165 mAh g^{-1} at 1C compared to 153 mAh g^{-1} at 20 °C, the cell cycled at lower temperature outperformed the one cycled at 40 °C after around 60 cycles. After 180 cycles, the cell cycled at 20 °C maintained a capacity of ca. 147 mAh g^{-1}, which is 15 mAh g^{-1} higher than for the cell tested at 40 °C (132 mAh g^{-1}).

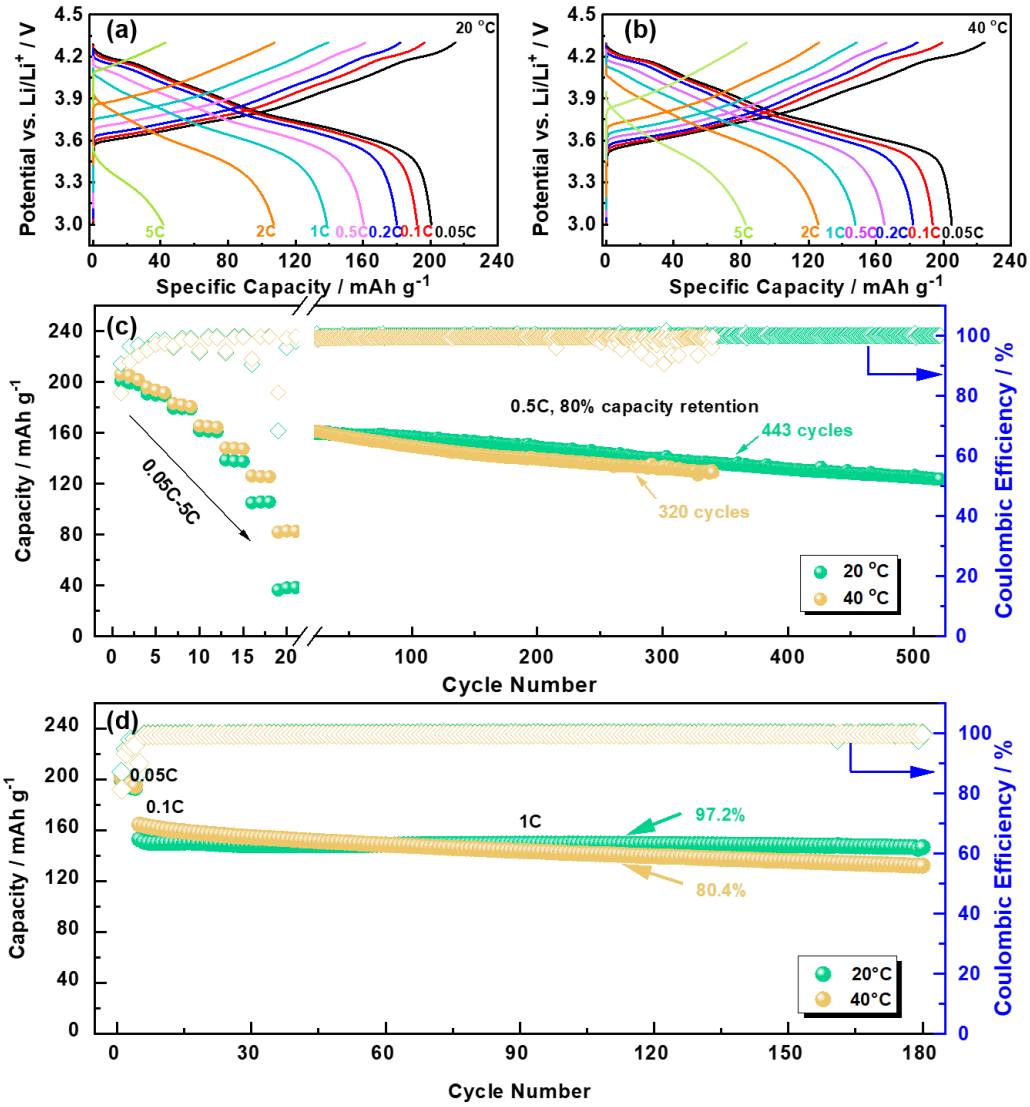

Fig. 4. Comparative rate capability test and constant current cycling of Li/SI10-05-70%PC/NCM_{811} cells at 20 °C and 40 °C. a,b) Selected dis-/charge profiles at varying C rates at a) 20 °C and b) 40 °C; c) Comparison of the rate capability (0.05C, 0.1 C, 0.2C, 0.5C, 1C, 2C, and 5C) and subsequent long-term cycling performance at 0.5C at both temperatures; d) Comparison of the constant current cycling performance at 1C for 180 cycles at 20 °C and 40 °C (the cut-off voltages were set to 3.0 V and 4.3 V).

3.5 The evolution of electrode kinetics upon cycling

In order to investigate the reason for this fading – though very limited at 20 °C, but pronounced at 40 °C – we conducted the same test again (*i.e.*, constant current cycling at 1C and 20 °C) and included electrochemical impedance spectroscopy (EIS) measurements after selected cycles in the discharged (*i.e.*, at 3.0 V) and charged (*i.e.*, at 4.3 V) states (Fig. 5). Since this test was conducted in two-electrode Swagelok-type cells (due to the difficulty to introduce a suitable reference electrode), the contribution of the Li metal anode is unavoidable. In the discharged (Fig. 5a) as well charged (Fig. 5b) states, the Nyquist plots for the selected cycles reveal a semicircle at higher frequencies. Considering that this feature varies upon cycling, but does not change with the cell's SOC (state of charge), and that lithiated NCM_{811} electrode generally exhibits a very small charge transfer impedance [50], we may assign the semicircle to the lithium metal/electrolyte impedance, which includes contributions from the charge transfer as well the solid electrolyte interphase [51]. For the first 10 cycles, this resistance is slightly increasing, presumably due to the reorganization of the lithium metal surface (solid electrolyte interphase) upon cycling [51]. For the subsequent cycles, however, it is continuously decreasing and eventually stabilizing after about 100 cycles, indicating a highly beneficial interface (and potentially an interphase) between the polymer-based electrolyte and the lithium metal electrode. At lower frequencies, a straight, but inclined line with a fixed frequency turning point of 17.5 Hz, is observed for the measurements performed on the cell in the discharged state (Fig. 5a), which is related to a diffusion process in the positive electrode (NCM_{811}) bulk. In the charged state (Fig. 5b) a second semicircle is observed instead, which is expected since the charge transfer resistance at the NCM_{811} electrode is not negligible in the delithiated state [50]. Different from the charge transfer resistance at the lithium metal electrode, this contribution to the overall impedance is increasing upon cycling until eventually stabilizing

after about 100 cycles. These results suggest that the critical point for further improvement is the stabilization of the interface (and potentially the interphase) at the positive electrode.

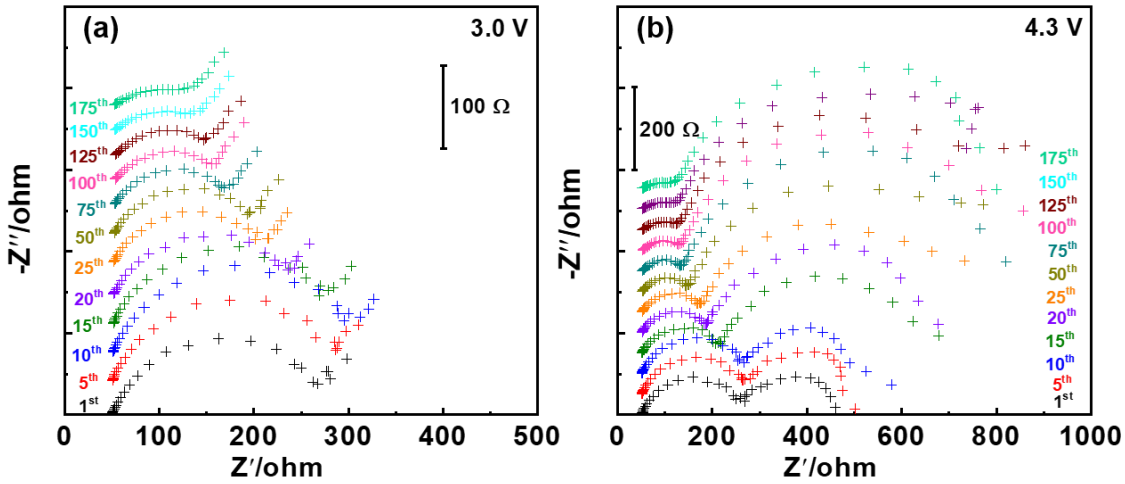

Fig. 5. Nyquist plots of the EIS data obtained for Li/SI10-05-70%PC/NCM_{811} full-cells cycled for 180 cycles at 1C and 20 °C in the a) discharged state (3.0 V) and b) charged state (4.3 V).

3.6 Morphology analysis of pristine and cycled electrodes

Nonetheless, the main goal of this study – the homogeneous wetting of the NCM_{811} active material particles and infiltration of the porous electrode – has been achieved, as apparent from the SEM/EDX analysis presented in Fig. 6. While the pristine electrodes generally show a good dispersion of the NCM_{811} active material, the PVdF binder, and the conductive carbon, they still provide several pores (indicated by the yellow circles in Fig. 6a,b) despite the pressing. These pores can be effectively filled by the optimized SI10-05-70%PC electrolyte, thus, achieving an intimate contact between the polymer-based electrolyte and the NCM_{811} active material particles without interfering with the percolating electronically conductive network of the carbon nanoparticles (Fig. 6c–l). In detail, Fig. 6c shows the bottom layer of the positive electrode after peeling off the aluminum current collector, revealing substantial amounts of the polymer-based

electrolyte, apparently in contact with the aluminum foil and homogeneously surrounding the NCM_{811} particles. An "inner" layer (*i.e.*, a layer closer to the lithium metal negative electrode, but not the outermost one, which we could not recover due to the intimate contact with the electrolyte) is presented from different perspectives and at different magnifications in Fig. 6d–f, confirming that the NCM_{811} particles are well embedded in and surrounded by the SI10-05-70%PC electrolyte. This homogeneous distribution of the polymer electrolyte is also evidenced by performing EDX analysis of a representative region (Fig. 6g) of the top layer of a cycled NCM_{811} electrode. Specifically, the sulfur mapping in Fig. 6l, which can solely result from the SI10-05-70%PC electrolyte, reveals a homogeneous distribution of the ionomer across the complete electrode surface. To further investigate the penetration of the polymer electrolyte into the NCM_{811} electrode, we also performed an EDX analysis of a representative region of the bottom layer of a cycled NCM_{811} electrode by removing the aluminum current collector (Fig. S5a). The elemental mapping of N (Fig. S5e), S (Fig. S5f), and F (Fig. S5g) reveals a high intensity for all these elements, indicating that the SI10-05-70%PC electrolyte has been successfully introduced into the porous electrode down to the bottom of the NCM_{811} electrode.

For the same cell, we managed also to recover the lithium metal electrode and conducted a comparative SEM analysis of the pristine lithium metal electrode and the cycled one (Fig. 7). While the former shows a very clean and smooth surface (Fig. 7a,b), the latter one reveals some surface roughening – without, however, any indication of dendritic lithium deposition (Fig. 7c,d). This is in very good agreement with the EIS results, suggesting a stabilized interface between the ionomer-based electrolyte and the lithium metal electrode after some initial surface reorganization and an increase in the total surface area; the latter is presumably causing the decrease of the charge transfer resistance.

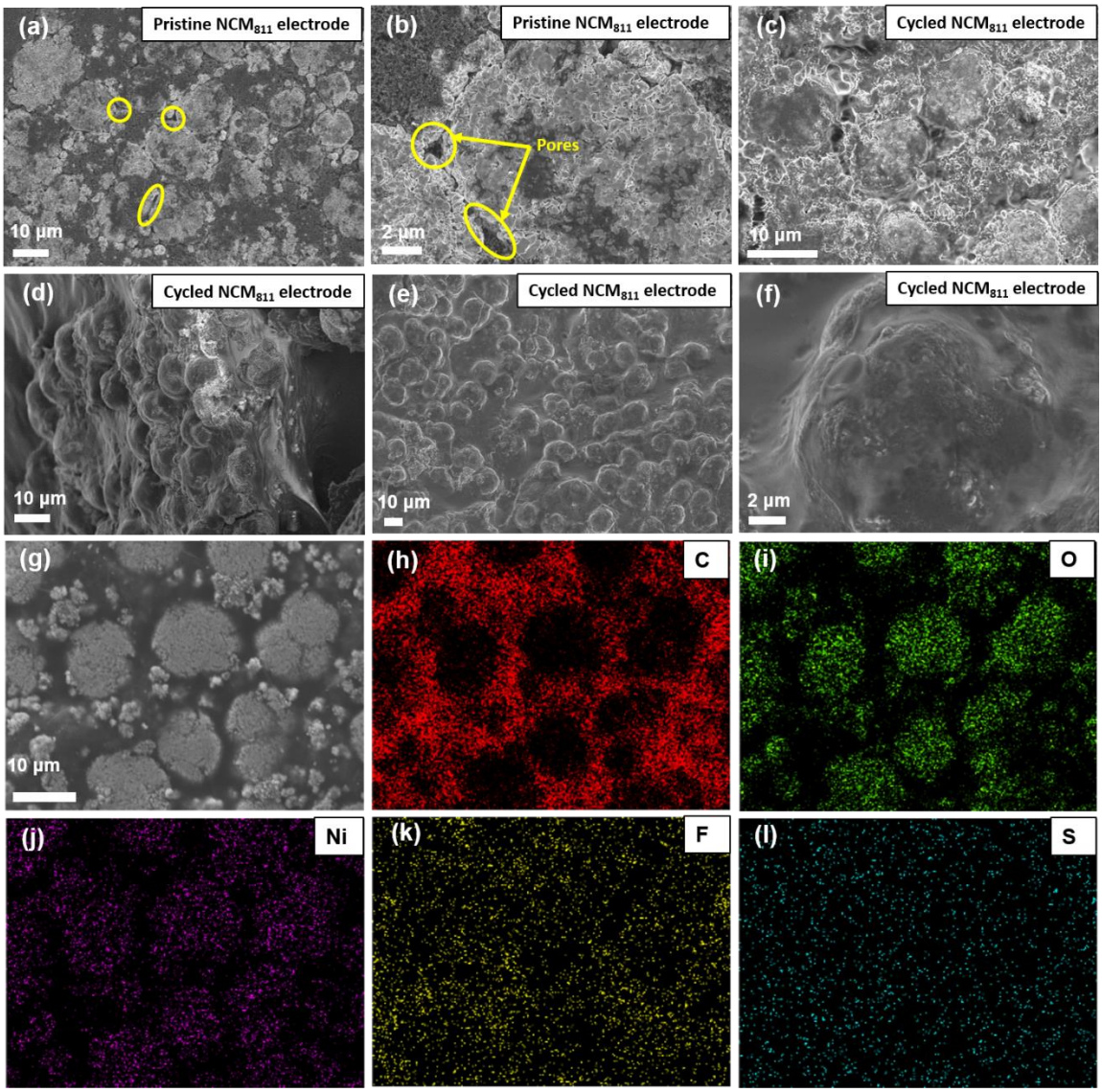

Fig. 6. Investigation of the NCM_{811} electrode morphology by SEM at different magnifications a,b) in the pristine state (*i.e.*, prior to the infiltration of the SI10-05-70%PC electrolyte) and c-f) after cycling at 20 °C (see Fig. 4c) comprising the SI10-05-70%PC electrolyte; note that c) shows the bottom layer of the NCM_{811} electrode after peeling off the aluminum current collector, while d) presents a view from the side at an "inner" layer of the electrode, which is moreover shown in the bird's eye view in e) and f) at different magnifications. g) SEM micrograph and h–l) EDX mapping of a cycled (top layer) NCM_{811} electrode (Fig. 4c at 20 °C) with the mapping of h) carbon in red, i) oxygen in green, j) nickel in purple, k) fluorine in yellow, and l) sulfur in turquoise.

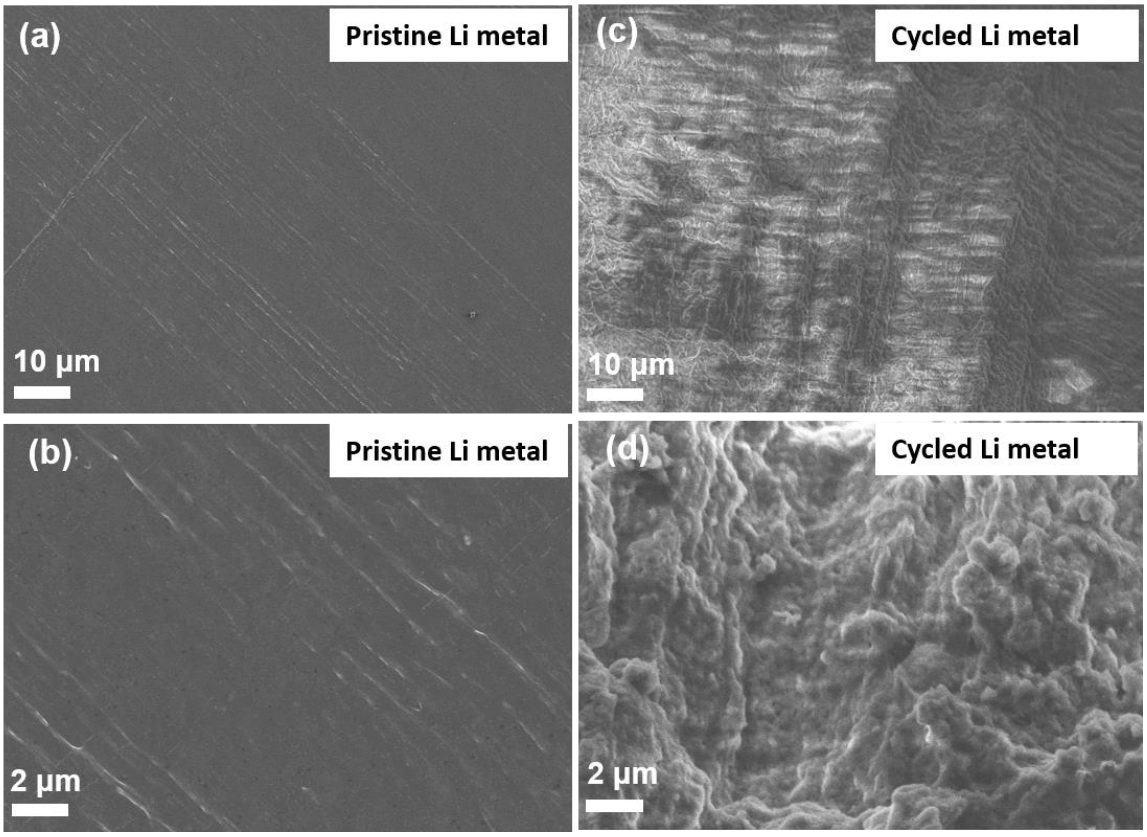

Fig. 7. Comparative SEM analysis at different magnifications of a,b) pristine lithium metal electrodes and c,d) cycled lithium metal electrodes (Fig. 4c at 20 °C).

3.7 Investigation of rate capability and long-term cycling performance under exertive conditions

Following this careful evaluation of the different interfaces and the infiltration of the NCM_{811} electrode by the SI10-05-70%PC electrolyte, we extended the electrochemical characterization of such Li/SI10-05-70%PC/NCM_{811} full-cells. In particular, to investigate the impact of the charging mode on the electrochemical performance, we added a constant voltage (CV) step (with a current cut-off of one tenth of the applied specific current) at the end of the constant current (CC) charging process (except for the initial formation cycles at 0.05C), commonly referred to CCCV cycling.

The comparative results for both temperatures (*i.e.*, 20 and 40 °C) are presented in Fig. 8a and Supplementary Fig. S6a,b. This modification of the charging mode allowed for achieving substantially higher capacities at all C rates, especially for dis-/charge rates above 0.5C. At 5C, for instance, the capacity increased from 38 mAh g^{-1} to 94 mAh g^{-1} at 20 °C and from 83 mAh g^{-1} to 135 mAh g^{-1} at 40 °C (Fig. 8a and Supplementary Fig. S6a,b). The relatively lower increase in case of 40 °C reflects the relatively lower impact of the additional CV step when the kinetics and Li^+ conductivity in the polymer electrolyte are already faster and the overall polarization is lower (Supplementary Fig. S6a,b). However, this improvement in rate capability is accompanied by a slightly inferior 80% capacity retention limit for the subsequent constant current cycling at 0.5C of 311 and 418 cycles at 40 and 20 °C, respectively (Fig. 8a).

An alternative approach to overcome the capacity decrease at elevated C rates, resulting from the increased polarization, is the increase of the anodic cut-off voltage. Moreover, performing a comparative investigation (20 °C) at elevated cut-offs, *i.e.*, 4.3 V, 4.4 V, and 4.5 V (Fig. 8b), allows us to explore the limits of the SI10-05-70%PC polymer-based electrolyte system. For the first cycle at 0.05C, the capacity increased slightly from 201 mAh g^{-1} (4.3 V; Supplementary Fig. S6c) to 204 mAh g^{-1} (4.4 V; Supplementary Fig. S6d) to 209 mAh g^{-1} (4.5 V; Supplementary Fig. S6e). The initial Coulombic efficiency, however, showed a reversed trend and decreased from 90.6% (4.3 V) to 88.1% (4.4 V) to 86.3% (4.5 V). The latter value, though, is still higher than for the first cycle at 40 °C with an anodic cut-off of 4.3 V, rendering such elevated cut-offs a viable strategy in general. When stepwise increasing the C rate, the capacity remains the highest for the anodic cut-off of 4.5 V until 0.5C (Fig. 8b and Supplementary Fig. S6f). At further increased C rates, however, it is only slightly superior compared to the anodic cut-off of 4.3 V, while the cell with an upper cut-off of 4.4 V clearly outperforms the latter two. The subsequent constant current

cycling reveals that the cell with the lowest anodic cut-off (4.3 V) provides the highest cycling stability with about twice the cycle number when the 80% capacity retention limit is reached (443 cycles *vs.* 226 cycles *vs.* 205 cycles for 4.3 V, 4.4 V, and 4.5 V, respectively). There is apparently an optimum to be found between the two goals of high rate capability and long-term cycling stability that would have to be implemented in the battery management system, *i.e.*, elevated cut-offs and potentially a CV step at elevated dis-/charge rates and lower cut-offs for the continuous cycling at relatively lower rates – depending also on the ambient temperature.

To further explore the latter also in the opposite direction, *i.e.*, towards lower temperatures, we subjected Li/SI10-05-70%PC/NCM_{811} full-cells to a rate capability test and subsequent constant current cycling at 0 °C (Fig. 8c). Due to the lower limiting current density at such low temperature (see Fig. 2b), we applied a maximum C rate of 2C, followed by 500 consecutive cycles at 0.5C (the latter is the same as for the previous tests). Remarkably, the Li/SI10-05-70%PC/NCM_{811} cell delivered rather high specific capacities also at 0 °C – specifically at C rates up to 0.5C – *i.e.*, 176 mAh g^{-1} at 0.05C, 161 mAh g^{-1} at 0.1C, 142 mAh g^{-1} at 0.2C, 109 mAh g^{-1} at 0.5C, 66 mAh g^{-1} at 1C, and 9 mAh g^{-1} at 2C. At least as remarkable is the subsequent long-term cycling stability at 0.5C for 500 cycles without any significant fading, accompanied by a high average Coulombic efficiency of 99.6%. This performance is, in fact, comparable to graphite/NCM_{424} full-cells comprising a standard liquid electrolyte composed of $LiPF_6$ and organic carbonates [52].

Finally, we conducted some mechanical deformation/abuse tests for the readily assembled Li/SI10-05-70%PC/NCM_{811} pouch cells by folding them and even cutting part of it (Video S4). The connected blue LED light does not stop working under such rather severe conditions, underlining the high reliability of such cells.

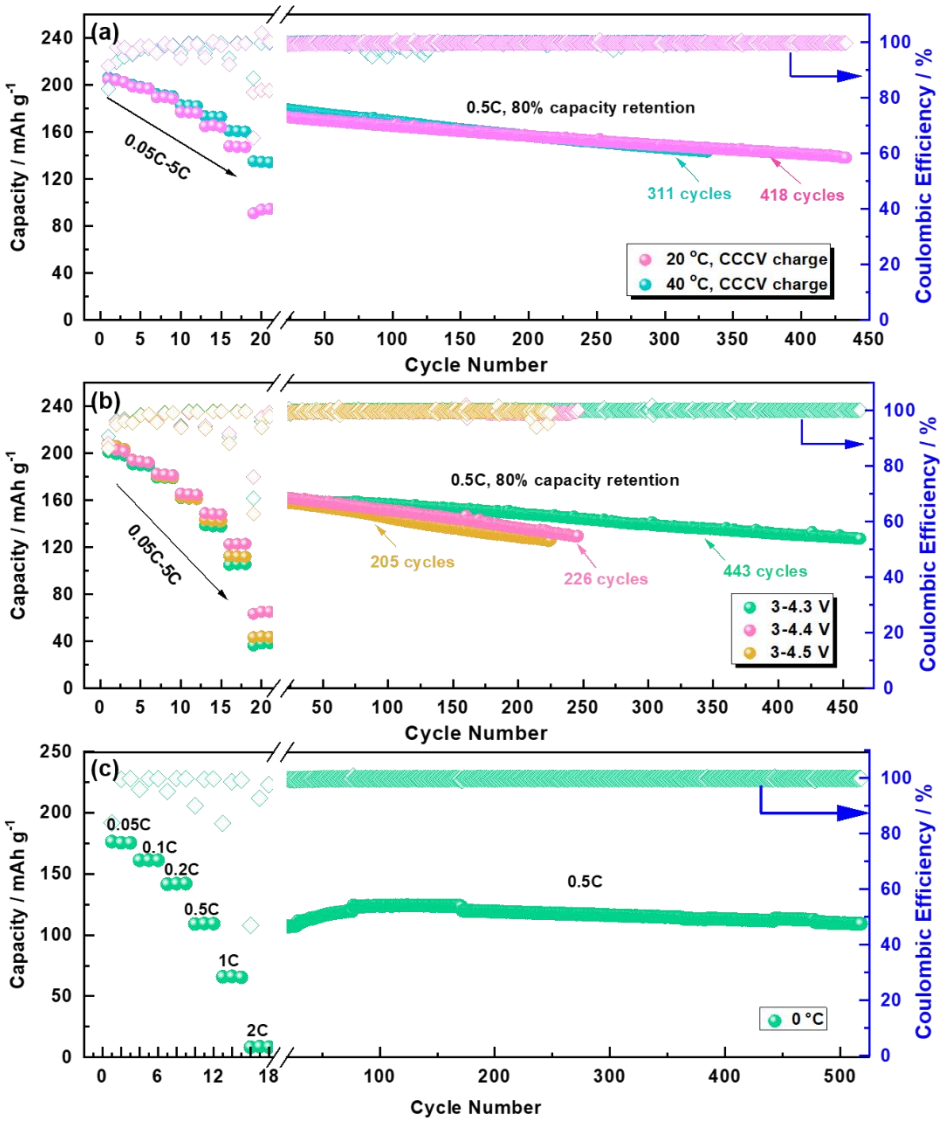

Fig. 8. a) Comparative investigation of the impact of a modified charging mode by introducing an additional constant voltage step (*i.e.*, CCCV cycling) on the rate capability and constant current cycling at 20 and 40 °C for Li/SI10-05-70%PC/NMC_{811} full-cells. b) Investigation of the effect of extending the upper cut-off voltage from 4.3 V to 4.4 V and 4.5 V on the rate capability and long-term constant current cycling of Li/SI10-05-70%PC/NCM_{811} full-cells. c) Investigation of the rate capability and long-term cycling performance of Li/SI10-05-70%PC/NCM_{811} full-cells at 0 °C (cut-off voltages: 3.0 V and 4.3 V).

4. Conclusions

Employing the optimized single-ion conducting multi-block copolymer electrolyte SI10-05-70%PC in Li/NCM_{811} cells allows for an excellent electrochemical performance of such next-generation lithium battery chemistry thanks to its high ionic conductivity, limiting current density, advanced de-/lithiation kinetics, and excellent stability towards oxidation and reduction as well as the successful infiltration of the NCM_{811} electrodes. While the cathode/electrolyte interface might be further stabilized in future studies – especially with regard to the elevated temperatures and anodic cut-off potentials as high as 4.5 V – these cells provide a remarkable rate capability and long-term cycling stability from more than 500 cycles even at 20 °C and 0 °C for carefully optimized charging modes. As this is, to the best of our knowledge, the first report on Li/NCM_{811} cells employing a single-ion conducting polymer electrolyte, we may anticipate that this work will trigger a further expanding interest in the development of safe high-performance and high-energy lithium-polymer batteries.

Acknowledgements

The authors would like to acknowledge financial support from the Federal Ministry of Education and Research (BMBF) within the FestBatt project (03XP0175B), the Helmholtz Association for basic funding, the French National Research Agency within the NSPEM project (ANR-16-CE05-0016), the Centre of Excellence of Multifunctional Architectured Materials “CEMAM” (AN-10-LABX-44-01), as well as the National Research Foundation of Korea (NRF) and the Korean government (MSIP; NRF-2018R1A4A1024691.

References

[1] M. Armand, J.M. Tarascon, Nature 451 (2008) 652–657.

[2] B. Scrosati, Garche, Jürgen, J. Power Sources 195 (2010) 2419–2430.

[3] D. Bresser, K. Hosoi, D. Howell, H. Li, H. Zeisel, K. Amine, S. Passerini, J. Power Sources 382 (2018) 176–178.

[4] B. Dunn, H. Kamath, J.-M. Tarascon, Science 334 (2011) 928–935.

[5] M.M. Thackeray, C. Wolverton, E.D. Isaacs, Energy Environ.Sci. 5 (2012) 7854–7863.

[6] J. Kalhoff, G.G. Eshetu, D. Bresser, S. Passerini, ChemSusChem 8 (2015) 2154–2175.

[7] Z. Chen, G.-T. Kim, Z. Wang, D. Bresser, B. Qin, D. Geiger, U. Kaiser, X. Wang, Z.X. Shen, S. Passerini, Nano Energy 64 (2019) 103986–103995.

[8] J. Liu, Z. Bao, Y. Cui, E.J. Dufek, J.B. Goodenough, P. Khalifah, Q. Li, B.Y. Liaw, P. Liu, A. Manthiram, Y.S. Meng, V.R. Subramanian, M.F. Toney, V.V. Viswanathan, M.S. Whittingham, J. Xiao, W. Xu, J. Yang, X.-Q. Yang, J.-G. Zhang, Nat. Energy 4 (2019) 180–186.

[9] X.-B. Cheng, R. Zhang, C.-Z. Zhao, Q. Zhang, Chem. Rev. 117 (2017) 10403–10473.

[10] X.-B. Cheng, R. Zhang, C.-Z. Zhao, F. Wei, J.-G. Zhang, Q. Zhang, Adv. Sci. 3 (2016) 1500213–1500232.

[11] M. Gauthier, A. Bélanger, P. Bouchard, B. Kapfer, S. Ricard, G. Vassort, M. Armand, J.Y. Sanchez, L. Krause, J. Power Sources 54 (1995) 163–169.

[12] H. Zhang, C. Liu, L. Zheng, F. Xu, W. Feng, H. Li, X. Huang, M. Armand, J. Nie, Z. Zhou, Electrochim. Acta 133 (2014) 529–538.

[13] D. Bresser, S. Lyonnard, C. Iojoiu, L. Picard, S. Passerini, Mol. Syst. Des. Eng. 4 (2019) 779–792.

[14] Y.S. Zhu, X.J. Wang, Y.Y. Hou, X.W. Gao, L.L. Liu, Y.P. Wu, M. Shimizu, Electrochim. Acta 87 (2013) 113–118.

[15] D. Zhou, D. Shanmukaraj, A. Tkacheva, M. Armand, G. Wang, Chem 5 (2019) 1–27.

[16] K. Jeong, S. Park, S.-Y. Lee, J. Mater. Chem. A 7 (2019) 1917–1935.

[17] M. Armand, Adv. Mater. 2 (1990) 278–286.

[18] C. Brissot, M. Rosso, J.N. Chazalviel, S. Lascaud, J. Power Sources 81-82 (1999) 925–929.

[19] M. Doyle, T.F. Fuller, J. Newman, Electrochim. Acta 39 (1994) 2073–2081.

[20] H. Zhang, C. Li, M. Piszcz, E. Coya, T. Rojo, L.M. Rodriguez-Martinez, M. Armand, Z. Zhou, Chem. Soc. Rev. 46 (2017) 797–815.

[21] R. Bouchet, S. Maria, R. Meziane, A. Aboulaich, L. Lienafa, J.-P. Bonnet, T.N. Phan, D. Bertin, D. Gigmes, D. Devaux, Nat. Mater. 12 (2013) 452–457.

[22] L. Porcarelli, A.S. Shaplov, F. Bella, J.R. Nair, D. Mecerreyes, C. Gerbaldi, ACS Energy Lett. 1 (2016) 678–682.

[23] R. Rohan, Y. Sun, W. Cai, Y. Zhang, K. Pareek, G. Xu, H. Cheng, Solid State Ionics 268 (2014) 294–299.

[24] R. Rohan, K. Pareek, Z. Chen, W. Cai, Y. Zhang, G. Xu, Z. Gao, H. Cheng, J. Mater. Chem. A 3 (2015) 20267–20276.

[25] H. Oh, K. Xu, H.D. Yoo, D.S. Kim, C. Chanthad, G. Yang, J. Jin, I.A. Ayhan, S.M. Oh, Q. Wang, Chem. Mater. 28 (2016) 188–196.

[26] C. Li, B. Qin, Y. Zhang, A. Varzi, S. Passerini, J. Wang, J. Dong, D. Zeng, Z. Liu, H. Cheng, Adv. Energy Mater. 9 (2019) 1803422–1803430.

[27] H.-D. Nguyen, G.-T. Kim, J. Shi, E. Paillard, P. Judeinstein, S. Lyonnard, D. Bresser, C. Iojoiu, Energy Environ. Sci. 11 (2018) 3298–3309.

[28] R. Petibon, J. Xia, L. Ma, M.K.G. Bauer, K.J. Nelson, J.R. Dahn, J. Electrochem. Soc. 163 (2016) A2571–A2578.

[29] L. Ma, S.L. Glazier, R. Petibon, J. Xia, J.M. Peters, Q. Liu, J. Allen, R.N.C. Doig, J.R. Dahn, J. Electrochem. Soc. 164 (2017) A5008–A5018.

[30] M. Metzger, C. Marino, J. Sicklinger, D. Haering, H.A. Gasteiger, J. Electrochem. Soc. 162 (2015) A1123–A1134.

[31] K. Xu, Chem. Rev. 104 (2004) 4303–4418.

[32] H.F. Mark, N.G. Gaylord, N.M. Bikales (Eds.), Interscience Publishers, New York 7 (1967) 24.

[33] M. Ciobanu, L. Marin, V. Cozan, M. Bruma, Rev. Adv. Mater. Sci. 22 (2009) 89–96.

[34] M. Bruma, O. Olabisi, O. Olabisi Dekker, New York (1997) 771–798.

[35] K. Borzutzki, J. Thienenkamp, M. Diehl, M. Winter, G. Brunklaus, J. Mater. Chem. A 7 (2019) 188–201.

[36] X. Wang, Z. Liu, Q. Kong, W. Jiang, J. Yao, C. Zhang, G. Cui, Solid State Ionics 262 (2014) 747–753.

[37] L. Porcarelli, A.S. Shaplov, M. Salsamendi, J.R. Nair, Y.S. Vygodskii, D. Mecerreyes, C. Gerbaldi, ACS Appl. Mater. Interfaces 8 (2016) 10350–10359.

[38] L. Porcarelli, M.A. Aboudzadeh, L. Rubatat, J.R. Nair, A.S. Shaplov, C. Gerbaldi, D. Mecerreyes, J. Power Sources 364 (2017) 191–199.

[39] Z. Shao, P. Jannasch, Polym. Chem. 8 (2017) 785–794.
[40] Q. Pan, Y. Chen, Y. Zhang, D. Zeng, Y. Sun, H. Cheng, J. Power Sources 336 (2016) 75–82.
[41] X. Zhang, R. Kostecki, T.J. Richardson, J.K. Pugh, P.N. Ross, J. Electrochem. Soc. 148 (2001) A1341–A1345.
[42] Y.T. Yuki Yamada, Kohei Miyazaki, and Takeshi Abe, J. Phys. Chem. C 114 (2011) 11680–11685.
[43] G.T. Kim, G.B. Appetecchi, M. Carewska, M. Joost, A. Balducci, M. Winter, S. Passerini, J. Power Sources 195 (2010) 6130–6137.
[44] S.T. Kiyoshi Kanamura, Soshi Shiraishi, and Zen-ichiro Takehar, J. Electrochem. Soc 143 (1996) 2548–2558.
[45] S.M. Cormac O. Laoire, and K. M. Abraham, J. Phys. Chem. C 114 (2010) 9178–9186.
[46] Q. Gan, N. Qin, Y. Zhu, Z. Huang, F. Zhang, S. Gu, J. Xie, K. Zhang, L. Lu, Z. Lu, ACS Appl. Mater. Interfaces 11 (2019) 12594–12604.
[47] P. Hou, H. Zhang, X. Deng, X. Xu, L. Zhang, ACS Appl. Mater. Interfaces 9 (2017) 29643–29653.
[48] Z. Chen, J. Wang, D. Chao, T. Baikie, L. Bai, S. Chen, Y. Zhao, T.C. Sum, J. Lin, Z. Shen, Sci. Rep. 6 (2016) 25771–25781.
[49] N. Elgrishi, K.J. Rountree, B.D. McCarthy, E.S. Rountree, T.T. Eisenhart, J.L. Dempsey, J. Chem. Educ. 95 (2017) 197–206.
[50] S.J. An, J. Li, D. Mohanty, C. Daniel, B.J. Polzin, J.R. Croy, S.E. Trask, D.L. Wood III, J. Electrochem. Soc. 164 (2017) A1195–A1202.
[51] G.B. Appetecchi, G.-T. Kim, M. Montanino, F. Alessandrini, S. Passerini, J. Power Sources 196 (2011) 6703–6709.
[52] Z. Chen, G.-T. Kim, D. Bresser, T. Diemant, J. Asenbauer, S. Jeong, M. Copley, R.J. Behm, J. Lin, Z. Shen, S. Passerini, Adv. Energy Mater. 8 (2018) 1801573–1801585.